Engineered Bio-Silver Nanoparticle Interface Offers Antimicrobial Properties

for Improved Cellular Viability

By

Sarah Kay VanOosten

Submitted to the graduate degree program in BioEngineering and the Graduate Faculty of the University of Kansas in partial fulfillment of the requirements for the degree of Master of Science.

_____

Chair: Dr. Candan Tamerler, Ph.D.

_____

Dr. Paulette Spencer, D.D.S., Ph.D.

_____

Dr. Malcolm L. Snead, D.D.S., Ph.D.

Date Defended: July 22, 2016

The Thesis Committee for Sarah Kay VanOosten

certifies that this is the approved version of the following thesis:

Engineered Bio-Silver Nanoparticle Interface Offers Antimicrobial Properties

for Improved Cellular Viability

_____

Chairperson Dr. Candan Tamerler, Ph.D.

Date approved: July 22, 2016

Abstract

Silver nanoparticles (AgNPs) are promising candidates for fighting drug-resistant infections because of their intrinsic antimicrobial effect. The antimicrobial efficacy, shown as a result of high-yield design of AgNPs, may inadvertently cause variation in host cells biological responses. While many factors affect AgNP efficacy, their surface is exposed to the biological environment and thus plays a critical role both in preserving antimicrobial efficacy against pathogens, as well as preventing cytotoxicity for host cells. Our approach for controlling nanoparticle surface properties is built upon engineering a biomimetic interface that provides a competitive advantage. Here, we engineered a fusion protein featuring a silver-binding peptide domain (AgBP) to enable self-assembly with green fluorescence protein (GFP) to track assembly. Following AgNP functionalization with GFP-AgBP, their antimicrobial properties were evaluated in conjunction with their cytotoxic properties. GFP-AgBP binding affinity to AgNPs was evaluated using localized surface plasmon resonance. The GFP-AgBP biomimetic interface on AgNP surfaces provided sustained antibacterial efficacy at relatively low concentrations based upon bacterial growth inhibition assays. As a test model, Streptococcus mutans was chosen as one of the common pathogens observed in dental caries. Viability and cytotoxicity measurements in fibroblast cells (NIH/3T3) exposed to protein-functionalized AgNPs showed significant improvement compared to controls. Biointerface engineering offers promise toward tailoring AgNP efficacy while addressing safety concerns to maintain optimum cellular interactions.

Acknowledgements

I would like to extend my overwhelming gratitude to the numerous mentors, family, and friends who have supported me throughout this process. To my advisor, Dr. Candan Tamerler, for her unyielding encouragement, patience, and guidance. To my committee members Dr. Paulette Spencer and Dr. Malcolm Snead who have also helped shape me into a better scientist. To my incredible family and all my relatives – my parents, Ann and Jim, and my brothers, Matthew and David – I am so lucky to be part of this family! To my loving boyfriend, Patrick, for being my rock and motivation. To my amazing friends for always being a shoulder to lean on – you've made me feel at home and been with me through the good days and bad. To the many mentors who have guided and inspired me – with a special thanks to Sathish, Annie, and Banu. To my many colleagues, lab-mates, and friends for all of your time, help, advice, ideas, and support.

Thank you. So very much.

This research was supported by NIH-National Institute of Arthritis and Musculoskeletal and Skin Diseases (NIAMS), AR062249-03 and NIH, National Institute of Dental and Craniofacial Research (NIDCR) R01DE025476-01and through NFR support provided through the University of Kansas.

Table of Contents

1. Chapter 1: Background & Significance

1.1 Background

1.1.1 Biomaterial-Associated Infections

The high rates of biomaterial-associated infections and the global healthcare burden associated with the increase in drug resistant bacteria have prompted significant efforts to develop effective antimicrobial agents.[1, 2], For the oral cavity, infections can occur in approximately 5% of implanted dental devices with these infections having broad adverse systemic impact.[3-6] In the USA, nearly 300,000 dental implants are placed each year to replace or restore craniofacial defects or missing teeth.[7] The high number of craniofacial infection is primarily attributed to poor material compatibility, the volatile environment with numerous oral bacteria and the formation of an impenetrable biofilm.[8, 9] These biofilms shield the bacteria from shear stresses, traditional antibiotics, and native immune responses, while simultaneously allowing some of the bacteria to escape and invade new surfaces at remote sites.[1, 10, 11] Antibiotic drugs relied upon to fight local and systemic infections are being undermined by bacterial resistance. Further, numerous authoritative health institutions have fervently informed the global population about the burgeoning threat and imminent health crisis regarding antibiotic resistant bacterial strains.[12-14] Each year, new antibiotic-resistant bacterial strains are identified and continue to grow at much faster rate than the pharmaceutical industry can develop novel antibiotics to combat them.[15] There has been an increasing significant effort to develop antimicrobial agents to combat drug resistant bacteria, while protecting patients from systemic infections and their consequences.

1.1.2 Silver Species: Alternative Antimicrobial Agent

Innovative approaches to biomaterial design for dental implants have focused on mitigating the risk of infection at the implant-tissue interface. Recent approaches are designed to coat or functionalize the implant surface with various antimicrobial moieties to create an anti-infective layer between the implant and native tissue.[11] Numerous antimicrobial moieties and device coatings have been clinically approved to combat the persistent and challenging burden of infections by either limiting bacterial adhesion or actively killing the bacteria upon direct contact.[16]

Silver species [17-35], metal oxides [36-43], various proteins and peptides [44-52], charged polymers [53-59], quaternary ammonium salts (QACs) [60-64], and selenium species [65, 66] are among the various agents which have been identified as promising weapons in this combat. Silver species and specifically silver nanoparticles (AgNPs), have received significant attention due to their distinctive physicochemical and antimicrobial properties. Prior to the introduction of antibiotics in the 1940's, silver was the most important antimicrobial agent in medicine, utilized for over six millennia to combat infection.[17] Even though silver has been used without any documented cases of bacterial resistance, cellular toxicity reports have triggered major safety concerns for AgNPs toward healthy tissue in humans. The antimicrobial efficacy and potential cytotoxicity of AgNPs *in vitro* has been shown to be highly dependent upon many factors including, but not limited to, nanoparticle size, concentration, stabilization, charge, or surface functionalization properties. The ability to tune and control the biological and biocidal effects is critical to determine an optimal compromise between maintaining antimicrobial properties while mitigating risk of adverse cytotoxic impacts. However this process is difficult as the exact mechanism by which AgNPs impart an effective antimicrobial properties remains largely unclear, although several groups have attempted to elucidate its mechanisms of action.[21]

1.1.3 Silver Nanoparticle Mechanisms and Characterization

A variety of potential mechanisms have been proposed, including silver ion release, cell membrane interaction and damage, disruption of both ATP synthesis and DNA replication, reactive oxygen species and further free radical generation.[19, 21, 67] Numerous studies have shown that the overall bactericidal efficacy is highly dependent upon the size and shape of the AgNPs used.[24, 26, 68-72] The general trend observed indicates that smaller size nanoparticles exhibit a more potent antimicrobial effect.[28, 72]

Martinez-Castanon, *et al*, show that minimum inhibitory concentration (MIC) of AgNPs on *Staphylococcus aureus* strains changes from 7.5 μg/mL to 16.67 μg/mL and eventually to 33.71 μg/mL as NPs' size changes from 7 to 29 and to 89 nm, respectively.[26] Most prior work performed on size-dependent antimicrobial effect of AgNPs was against *Escherichia coli* as a test bacterial strain. However, with rising interest to the oral microbiome and bacterial related caries studies,[73] many groups started to focus on oral pathogens since dental caries remains the most prevalent infectious disease of mankind.[74] For one of the most abundant oral pathogens, *Streptococcus mutans*, the size-dependent effect was shown for NPs of 8.4, 16.1, and 98 nm, where the MIC changed correspondingly to 102, 146 and 320 μg/mL, respectively.[22] The same trend was also recently shown on a different oral pathogen strain, where the smallest size NP's (5nm) was found to have the largest antimicrobial effect.[24] For example, for *S. mutans* and *Streptococcus sanguis,* an MIC of 100 μg/mL was observed for 5nm AgNPs compared to a MIC of 200 μg/mL in the case of 55 nm AgNPs.[23]

Size dependence of activity may be explained by one mechanisms of AgNP action against bacteria, namely, the interaction of the particle with the bacterial cell membrane with the consequential reduction in cell membrane permeability and respiration. In this case, the smaller size particles have a greater ability to cover a larger area of the membrane, thus having a more potent effect on altering vital cellular functions.

Silver nanoparticles have also been applied to combat bio-film formation associated with dental caries, where they have been evaluated for their cytotoxic effect on local tissue and host cell integrity. Size-dependent cytotoxic effects have also been observed by several groups.

Hernandez-Sierra, *et. al.*, have investigated the cytotoxic effects of AgNPs, sized 10, 20, and 80 nm, on local dental tissues, evaluated following exposure times of 1, 3, and 7 days.[23] Results indicated that AgNPs 20nm or smaller increased cytotoxicity in both a time and dose dependent matter, when compared to 80-100nm-sized AgNPs which did not significantly modify the viability of primary human culture cells.[23] Therefore, an optimal AgNP size is dependent upon its intended use and application, where a balance must be established to select an Ag particle size at which the antimicrobial properties are maintained, while cytotoxic effects to host cells are mitigated. AgNPs with a size range of 10–25 nm were reported to be more likely to promote cellular apoptosis, as well as increased ROS production, when compared to larger AgNPs with a size of 80 nm.[75] Results measuring the cytotoxic effects of 10nm AgNPs on epithelial lung cells were shown to be surface-coating independent, when compared to AgNPs sized 40 and 75 nm.[71] However, it has been concluded that easier uptake and larger surface area for AgNPs can serve to make smaller nanoparticles more toxic.[24] In contrast, a study by Arora, et. al., suggested that following the uptake of selected concentrations of NPs sized 7–20 nm, the antioxidant mechanisms found in eukaryotic cells can prevent further oxidative damage from the particles.[76] Another group reported that 200 μM of 20 nm silver nanoparticles did not induce cytotoxic effects in human dermal fibroblast cells after incubation for up to 8 hours.[77] Interestingly, in another study reported a subsequent apoptosis of a fibroblast cell line treated with 1-100 nm-sized AgNPs.[78]

Due to these contradictory reports, it is critical to also investigate surface functionalization techniques as a way to mediate antimicrobial properties and cytotoxicity.

1.1.4 Silver Nanoparticle Functionalization

AgNP functionalization and its consequential effect on particle stabilization has been shown to alter cytotoxicity.[47] Coating or functionalizing AgNPs surfaces with polymers or biomolecules, including proteins, alters AgNP size and properties due to the formation of a coronal structure formed upon subsequent contact with biological fluids from host tissues.[3, 44, 47, 50, 79] Hard and soft coronal structures and compositions alter the AgNP structure and size and therefore can affect the both their innate antimicrobial properties and cellular cytotoxicity.[47, 49] The effects of the transient, soft corona layer on AgNP function and cellular uptake have not yet been studied in detail due to the inability to accurately distinguish the rapidly exchanging, weakly-bound proteins in various biological environments.[79] However, the sustained complex protein corona properties have been linked to nanoparticle aggregation and cellular association.[50, 79] Agglomeration substantially reduces the antimicrobial capacity of AgNPs, so maintaining a dispersed and stable AgNPs population is critical. There is strong evidence that different protein components existing in biological environments may compete for the AgNP surface and create a secondary protein corona signature. The complex protein corona composition of AgNPs in the host cell environment may trigger different biological responses; the biological responses may affect cellular and biophysicochemical mechanisms, which are of utmost importance for deciphering and addressing the safety concerns associated with the use of AgNPs as antimicrobial agents.

1.2 Innovation and Approach

In the scope of this work, we explore the development of a robust, biomimetic surface functionalization approach onto AgNPs using engineered fusion proteins that have the ability to self-assemble at the material interface through their genetically engineered silver binding peptide tags (AgBP).

In our previous work, we have designed a multifunctional fusion protein, which included a green fluorescence protein (GFP) and a silver-binding peptide (AgBP), identified using phage display technology.[48] We demonstrated that the AgBP tag directs the fusion protein to self-immobilize selectively onto silver nanoparticle arrays on ferroelectric materials.[80] Herein, we explored this approach as a way to fight infection and therefore we investigated he bactericidal and cytotoxic effects of the fusion-protein stabilized silver nanoparticles.

We first investigate the binding strength and stability of the fusion protein to the nanoparticles using localized surface plasmon resonance sensing (LSPR). With the notable selective binding obtained at the nanoparticle interfacial surface, we next explored the antimicrobial effect of the fusion protein coated particles on *Steptococcus mutans* bacterial strain as one of the common pathogen in dental caries. Encouraged with the minimum inhibition concentration obtained with relatively low AgNP concentration, we next demonstrated a significant reduction in cytotoxicity effects on fibroblasts cells and in addition observed an improved metabolic activity for treated cells compared to control AgNPs. The biomimetic surface approach described here could be expanded to any other nanoscale material surfaces where specific inorganic binding peptides could be engineered into proteins and peptides. This enabling technology builds upon biological self-assembly that is driven by molecular recognition of the material surfaces by short peptides. This biomimetic interface approach may a way to overcome safety concerns in next generation biomaterials by bringing in a competitive advantage at the bio-material interfaces to tailor desired bioactivity.

.

2. Chapter 2: Materials and Methods

2.1 Production of GFP-AgBP Fusion Protein

MBP-GFP and MBP-GFP-AgBP proteins were expressed and purified as previously described.[48, 81] Briefly, following protein expression, cells were harvested via centrifugation at 4000 rcf for 30 minutes. Cell pellets were re-suspended in column buffer (20mM Tris-HCl, 200mM NaCL, 1mM EDTA, pH 7.4). Cells were disrupted via sonication and cell debris was removed by centrifugation. Supernatant was loaded onto a buffer-equilibrated amylose resin column (New England Biolabs, NEB) and washed to remove unbound protein. MBP-tagged proteins were eluted using column buffer supplemented with 10mM maltose. Pure protein fractions were concentrated to 1 mg/ml using Amicon Ultra-15 centrifugal filters (Millipore) and transferred to a cleavage buffer (20 mM Tris-HCl, 100 mM NaCl, and 2 mM CaCl2, pH 8.0).

The MBP tag was enzymatically removed using 30 µl of 1 mg/ml Factor Xa (NEB) added to 2.5 mg/ml fusion protein substrate. The reaction was incubated at 16°C overnight under gentle agitation. Each fusion protein cleavage mixture was loaded onto a hydroxyapatite (BioRad) column equilibrated in 20 mM sodium phosphate and 200 mM NaCl (pH 7.2) buffer. After maltose molecules were washed away, protein samples were eluted with 0.5 M sodium phosphate (pH 7.2). Hydroxyapatite-eluted protein samples were next loaded onto a regenerated amylose resin column. MBP-free protein samples were collected as the flow-through. Protein purity was assessed using SDS-PAGE gel electrophoresis.

2.2 Silver Nanoparticle Functionalization

Stock, citrate-coated silver nanoparticles (AgNPs) sized 20, 40, and 80nm (Ted Pella) were diluted to desired concentrations. 40nm AgNPs were selected as the most ideal size for detailed analysis, reported herein, following initial experimental results on cellular cytotoxicity and

bactericidal efficacy. The stock concentration for the 40nm AgNPs was provided as 0.024 mg/ml of silver. AgNPs were incubated with a range of protein concentrations for both GFP and GFP-AgBP. AgNPs were diluted from the stock in DI water and allowed to mix with protein for 24 hours at room temperature with gentle agitation.

The binding affinity and stability of the engineered bi-functional protein, GFP-AgBP, onto AgNPs was studied using localized surface plasmon resonance (LSPR). AgNPs were diluted in DI water from the stock to achieve a final concentration of 40 μM. A range of protein concentrations of either GFP alone or GFP-AgBP were compared to AgNPs diluted in DI water only. LSPR was performed on AgNPs prior to exposure to proteins or water control. Following a 24 hour incubation time, absorbance spectra were taken to study spectral peak shifts due to changes in AgNP size or shape, and again following a wash step. Washes were done for all AgNP samples by pelleting via centrifugation for 30 minutes at 3000 rcf. The supernatant was carefully collected to remove unbound proteins and AgNPs were then reconstituted in DI water and subjected to final LSPR analysis.

AgNP functionalization for antibacterial and cellular viability studies were performed under similar conditions. Stock, citrate-coated 40nm AgNPs were diluted to 2X final concentrations desired and incubated with 40 μM GFP-AgBP functional peptide or in water only for 2 hours at room temperature with gentle mixing (the 2 hour incubation time was selected following time dependent binding analysis, not reported herein). Each sample was then pelleted via centrifugation and re-suspended in either BHI media or DMEM media for use in bacterial assays or fibroblast cellular viability assays, respectively.

2.3 Antimicrobial Activity Assays

The antimicrobial activity the GFP-AgBP-functionalized and citrate-coated AgNPs was studied in *Streptococcus mutans* (*S. mutans*; ATCC 25175) bacterial strain. The lyophilized

bacteria were reconstituted in Brain Heart Infusion medium (BHI; BD Difco), consistent with ATCC standard protocol, and streaked onto a BHI agar (BD Difco) plate. *S. mutans* plate was incubated for 24 hours at 37°C and in the presence of 5% CO_2. Overnight cultures were prepared prior to each experiment by inoculating 10 ml of fresh BHI media with a single colony of bacteria and incubating for 16 hours. The *S. mutans* cultures were then diluted and growth was monitored via optical density measurements at 600nm on a Cytation3 Imaging Multi-Mode Plate Reader (BioTek) until a final concentration of 10^7 colony forming units (CFU)/ml was reached.

Bacterial disc diffusion assay was carried to test the antimicrobial effect of nanoparticles. BHI agar plates were prepared and stored at 4°C and allowed to acclimate to room temperature 30 minutes prior to experiments. 10^6 CFUs of *S. mutans* were spread onto a pre-prepared BHI agar plate using aseptic technique. After 5 minutes, loaded discs were placed into each labeled quadrant of the plate. Porous, 30µm polyethylene filter discs were utilized to allow for uninhibited AgNP diffusion. Each disc was soaked in desired concentrations of protein-stabilized AgNPs and compared to the corresponding concentrations of the stock, citrate-coated AgNPs. A positive control of 10 µg/ml Ampicillin (Sigma) in DI water was employed and DI water was used as a negative control. Following placement of the discs, *S. mutans* plates were incubated for 24 hours at 37°C with 5% CO_2. The average diameter of the inhibition zone around each disc was measured using a digital calipers at various angles. The measured disc diameter was subtracted from the average zone of inhibition calculated for each treatment to normalize measurements for data analysis and representation.

Duplicate samples were prepared for each AgNP concentration studied. Experiments were repeated three times, each assay using a *S. mutans* grown from a different individual colony.

2.4 Cellular Cytotoxicity Assays

The murine-derived fibroblast cell line NIH/3T3 (ATCC CRL-1658) was used as a preliminary model to determine any effects the functionalized AgNPs had on cellular viability and cytotoxicity. Culture conditions followed ATCC protocol and previously established methods. Briefly, cells were grown at 37°C, supplemented with 5% CO_2 in Dulbecco's Modified Eagle's Medium (DMEM; ATCC 30-2002) containing 10% fetal bovine serum (FBS; Gibco) and 1% penicillin-streptomycin (Gibco). Media was changed the day after plating as well as media changes every 48 hours, as needed. Cells were sub-cultured at 80% confluency or biweekly with 0.25% Trypsin-EDTA (Gibco).

To follow cellular viability, NIH/3T3 cells were first seeded into 96-well plates with black side/clear (BrandTech) at 10^4 cells/well. Following complete cell attachment to plate, media was changed and various concentrations of untreated (stock, citrate-coated) and GFP-AgBP protein-functionalized AgNPs were added to each well and allowed to incubate for 24 hours at 37°C with 5% CO_2. To evaluate cellular viability, 10% v/v of AlamarBlue reagent (Life Technologies) was added to each treated well at the 22 hour time point, allowing cells to metabolize the reagent for about 2 hours prior to the 24 hour time point. Both absorbance and fluorescence measurements were recorded, according to company protocol, to quantitatively assess cellular viability following 24 hours of incubation with AgNP treatments.

Cellular viability and cytotoxicity was also quantified using Live/Dead Viability/Cytotoxicity Kit (Life Technologies) to indicate intracellular esterase activity and plasma membrane integrity. Cells were plated and treated in 96-well plates following the same protocol as above. Following a 24 hour incubation, cells were imaged using both brightfield and fluorescence imaging (BioTek Cytation3) to observe cell morphology and quantify cellular viability/cytotoxicity, respectively. Calcein-AM (green-fluorescent) stain identified healthy, viable cells whereas Ethidium Homodimer-1 (red-fluorescent) labeled the loss of membrane integrity of dead cells. Images were

taken for each well to determine the fluorescent contribution of the GFP-containing protein prior to Live/Dead staining and were subtracted for accurate staining activity analysis. Plates were treated such that 8 repeats of each AgNP concentration were averaged and compared to respective cell-only controls. A minimum of three plates were used for each concentration and treatment for analysis and normalized to respective plate controls. All results are presented as a mean ± standard deviation.

3. Chapter 3: Results and Discussion

The schematic drawing shown in Figure 1 demonstrates the multifunctional fusion protein approach described in this work. Here, we developed a stable biointerface built upon self-assembly of green fluorescence protein (GFP) engineered to include a silver binding peptide (AgBP) to produce multifunctional fusion protein that assembles on the surface of a silver nanoparticle. The AgBP provides a stable orientation for the GFP protein assembly on the AgNP surface as shown using localized surface plasmon resonance sensing. Next, AgNPs engineered with a biointerface, formed by the multifunctional fusion protein, are tested for antimicrobial activity over a range of concentrations and compared with the properties for widely accepted citrate-coated AgNPs. Achieving a similar concentration range for antimicrobial activity of engineered biointerface AgNPs, cytotoxicity and cell viability assays were carried out to compare the outcomes with both citrate coated and nonspecific protein coated AgNPs.

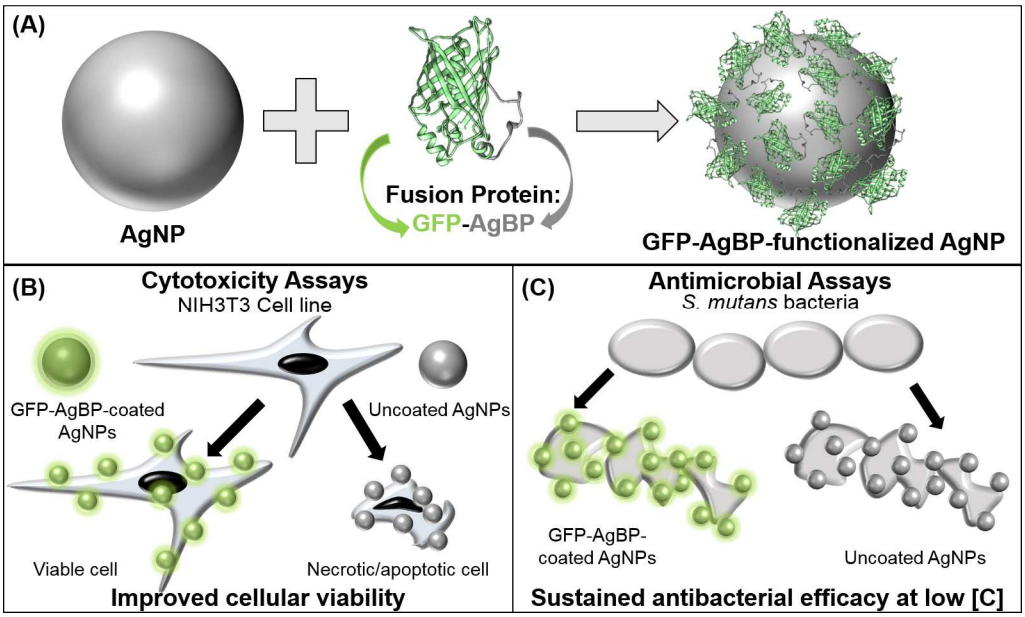

Figure 1. Schematics demonstrating the GFP-AgBP functionalization of silver nanoparticles (A), and the observed improvement in cellular viability *in vitro* (B) while maintaining the inherent antibacterial efficacy (C) at relatively low concentrations.

3.1 Characterization of Silver Nanoparticles

The phenomenon of surface resonance was used to monitor AgNPs, where light spectral scanning at 300-700nm resulted in a strong absorption peak at around 410nm. The binding affinity and stability of the engineered bi-functional protein, GFP-AgBP, onto AgNPs was studied using localized surface plasmon resonance (LSPR) and compared against AgNPs incubated with GFP protein alone (no silver affinity tag) (Figure 2).

LSPR spectra were taken to determine if protein binding was specific and stable following a wash step. AgNPs have unique interactions with light and display a characteristic optical spectra dependent upon their size and shape.[34, 79] Spectral shifts indicate an altered surface structure and size when AgNPs are successfully functionalized.[82] Silver nanoparticles did not result in agglomeration as an indication of instability of the interfaces at the reported concentration ranges and the nanoparticles sizes, they rather provided a distinct peak at the expected wavelength range. Greater adsorbed protein concentration resulted in a greater red-shift of the spectra, suggesting a slightly thicker nanoparticle size due to the relatively more stable protein layer formed at the surface. Additionally, the distinct peaks observed for both the GFP-coated and GFP-AgBP-functionalized AgNPs indicate the particles remained discrete and did not agglomerate at concentrations studied.

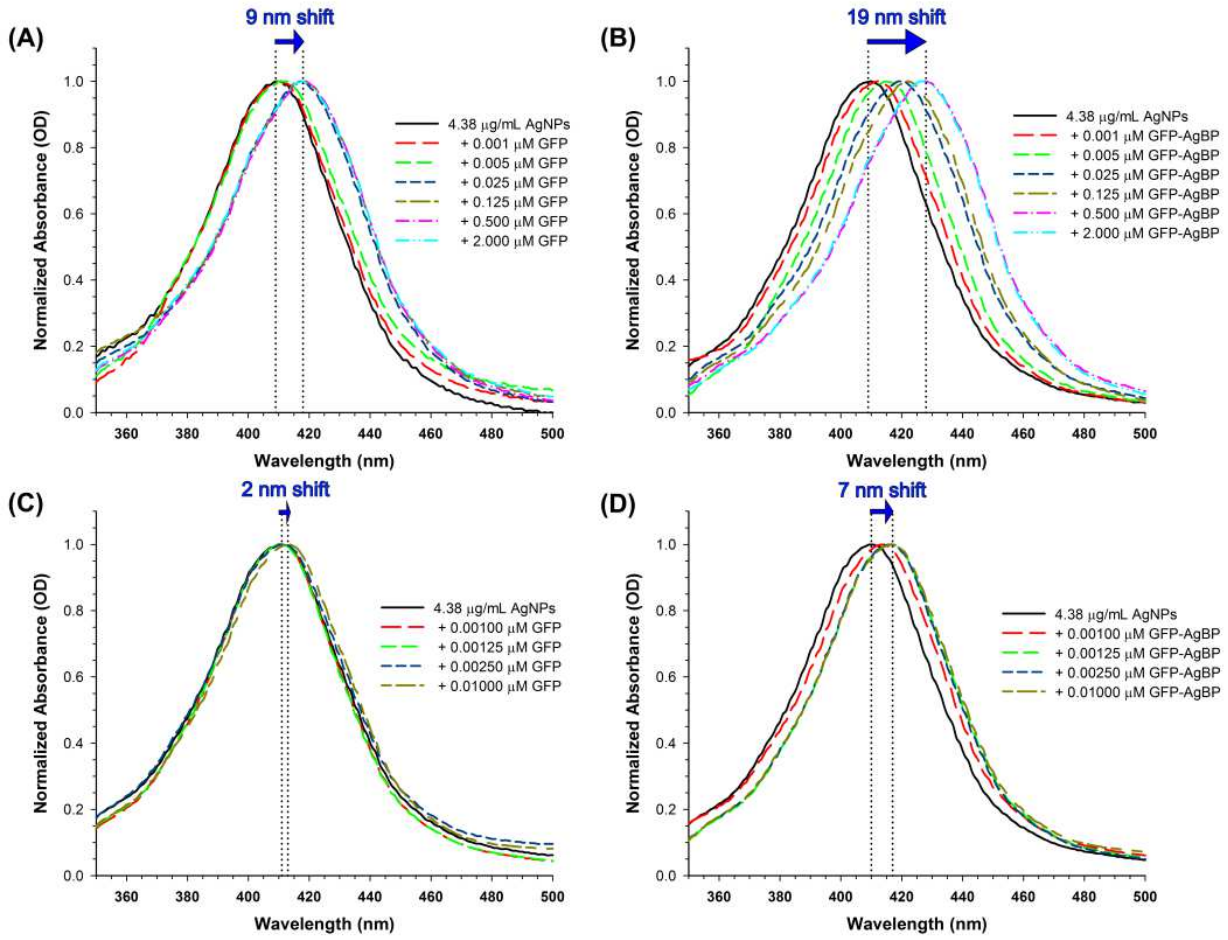

Figure 2. Localized surface plasmon resonance (LSPR) spectra to confirm protein functionalization on the AgNPs. LSPR spectral peaks collected after 24 hour of incubation with GFP wild type protein (A) and engineered bifunctional protein GFP-AgBP (B). A red-shift is observed as protein concentration increases. LSPR shifts following the 24 hour incubation and wash step to remove unbound (or weakly bound) protein indicate a sustained 2 nm shift for GFP (C) and a 7 nm shift for the GFP-AgBP spectra (D). GFP-AgBP is shown to provide a more stable and robust affinity AgNP coating when compared to the wild type protein alone.

Following a 24 hour incubation, 40 nm AgNPs coated with either GFP or GFP-AgBP proteins revealed maximum red-shifts in the spectra of 9 nm and 19 nm, respectively as compared

to untreated (stock, citrate-coated) controls with an average spectral peak of 409 nm (Figure 2a,b). Weakly bound and/or excess protein was then washed away with water. For concentrations less than 0.01 μM or less of proteins, a distinct peak was still observed following the wash step. LSPR spectra following the wash step displayed a spectra peak red-shift of only 2 nm and 7 nm for AgNPs coated with GFP and GFP-AgBP, respectively, as compared to untreated control samples (Figure 2c,d). The 7 nm shift observed for the GFP-AgBP-functionalized AgNPs indicates that the silver-binding affinity tag (AgBP) of our engineered fusion protein produces a stable and robust protein layer around the AgNPs as compared to the non-specific binding using GFP protein alone. These observations are consistent with recent literature findings for AgNP functionalization monitored by UV-vis absorbance red-shift due to dampened surface plasmon resonance.[34, 47, 83]

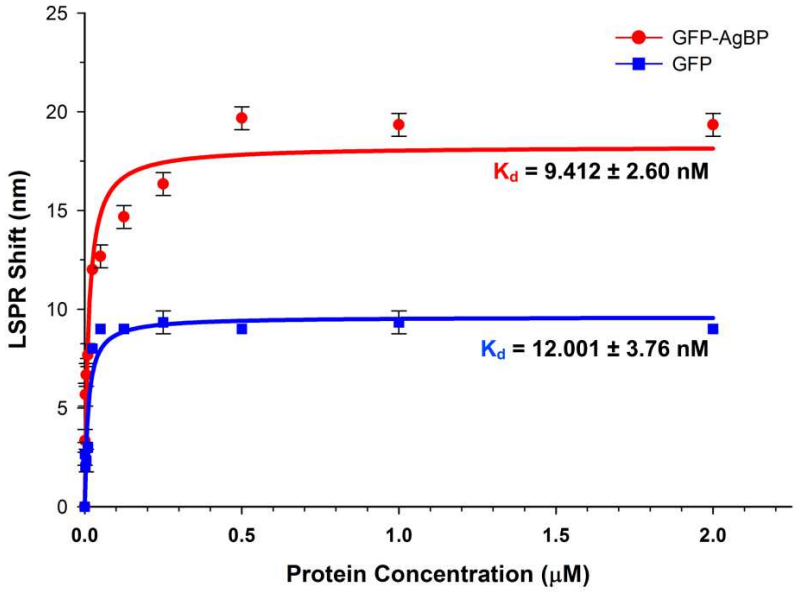

Figure 3. Specific binding fit analysis for averaged LSPR shifts obtained at different protein concentrations for GFP-AgBP and GFP proteins. Dissociation constant (Kd) values were calculated as about 9.4 and 12.0 nM for AgNPs coated with either GFP-AgBP or GFP wild type protein, respectively.

LSPR experiments run at different protein concentration were used to calculate the K_d values (dissociation constant) to compare quantitatively the protein binding affinity onto the nanoparticle surface (Figure 3). Looking at specific saturation binding in this approach, we used a Langmuir adsorption model equation (Equation 1) to study the curve fit to determine the K_d.

Equation 1: $$y = \frac{B_{max} * x}{K_d + x}$$

In Equation 1, the LSPR shift, y, was normalized from raw data by subtracting the peak wavelength of AgNPs alone (no protein) to determine the absolute shift in the peak absorbance following LSPR experiments at corresponding protein concentrations, x. The maximum LSPR shift at saturation, B_{max}, is calculated through the curve fit analysis. The dissociation constant, K_d, represents the concentration needed to achieve a half-maximum binding at equilibrium, thus a smaller value indicates a greater binding affinity which was validated by the fact our GFP-AgBP protein had a smaller Kd value than GFP wild type at about 9.4 nM and 12 nM, respectively. This data shows that by attaching a small, silver-binding protein we can enhance our specific binding to the silver nanoparticle surfaces.

3.2 Antimicrobial Efficacies of Silver Nanoparticles

The antimicrobial efficiency of the functionalized AgNPs was studied using growth inhibition models and disc diffusion assays. Figure 4a shows a representative plate from the disc diffusion assay experiments. Clearly-observed zones of growth inhibition are seen the 40 nm AgNPs, as compared to a control (water only) disc. Figure 4b indicates a trend which suggests AgBP-GFP-functionalized nanoparticles may have an enhanced antimicrobial efficacy, although it was not statistically significant across all concentrations tested. The zones of inhibition were statistically similar for concentrations of 1.31, 2.63, and 5.25 µg/ml for the citrate-coated control and protein-functionalized samples (Figure 4b). At the lowest concentration, 0.66 µg/ml, the GFP-

AgBP functionalized AgNPs showed a significantly larger zone of inhibition as compared to control nanoparticles. This difference can be attributed to the fact that the protein-coated nanoparticles boasted a stable biomimetic interface compared to the citrate-coated controls, allowing them to diffuse more easily from the loaded disc even at low AgNP concentrations. These data indicate that our protein-functionalized AgNPs potentially provide more potent and effective antimicrobial properties. The measured zones of inhibition showed an increasing trend, but did not significantly change across concentrations of 1.31 µg/ml to 5.25 µg/ml. At higher concentrations, AgNPs have a greater potential to agglomerate, based upon spatial constraints in the treatment wells where the discs were pre-soaked in specified solutions and may get trapped or stuck to the polyethylene discs. Therefore, we attribute this plateau trend in inhibition zone at increasing AgNP concentrations to reduced diffusion capabilities for the concentrations of AgNPs we studied.

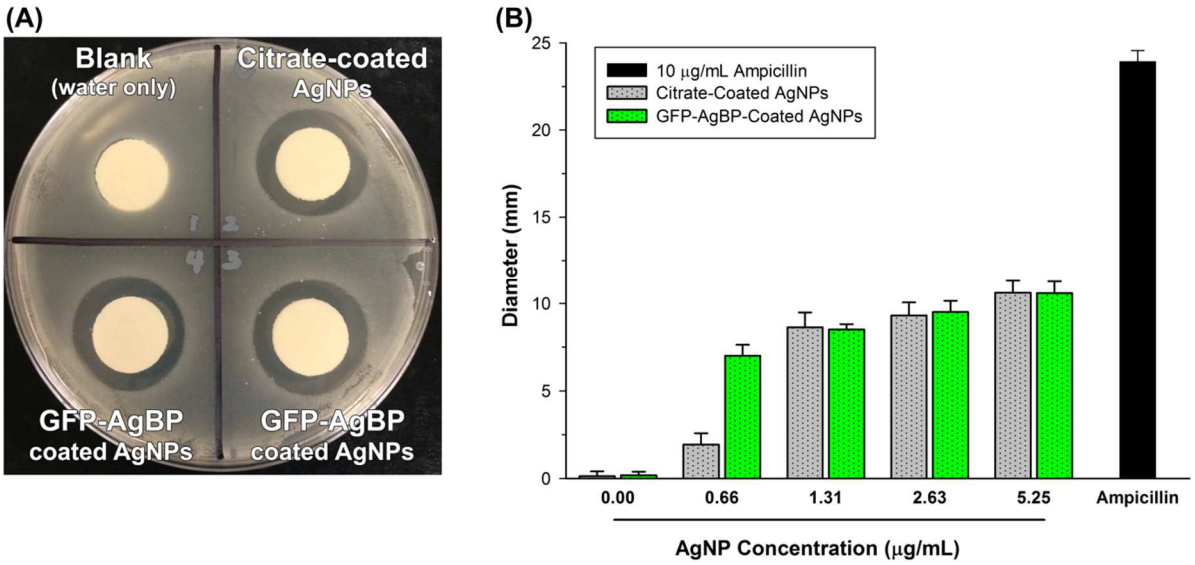

Figure 4. *S. mutans* Agar Diffusion Assay. Representative image for observed zones of inhibition for the 2.63 µg/mL AgNP concentration (A) comparing GFP-AgBP-coated AgNP loaded discs (duplicate samples shown) and citrate-coated AgNPs discs with respect to a blank control. Graphical representation for measured inhibition zone diameter across four different concentrations studied to compare AgNPs coated with GFP-AgBP or citrate (stock AgNPs) (B). Ampicillin (10 µg/mL) was loaded onto a disc as a positive control. Data

trend indicates enhanced antimicrobial function with increasing AgNP concentration for both coatings. GFP-AgBP-coated silver nanoparticles have a significantly greater antimicrobial effect than citrate-coated AgNPs at the lowest concentration studies (0.66 µg/mL).

It is important to note that this engineered protein coating does not limit the natural antimicrobial efficacy of silver nanoparticles. Numerous reports in the literature utilizing a variety of chemically and covalently attached polymers or biomolecular moieties to functionalize and stabilize AgNPs, also showed changes and an overall reduction in antimicrobial efficacy due to the functionalization technique.[83-86] However, in light of recent findings regarding protein corona formation and altered size effects of AgNPs, the thickness and chemical properties imparted by the coatings can lead to significant changes in cellular cytotoxicity. Our protein self-assembly technique provides a biologically tailored approach to functionalize nanoparticles with tunable and predictable surface properties while still maintaining the inherent antimicrobial functionality of AgNPs.

3.3 In vitro *Fibroblast Cellular Viability Model*

The effects of the protein-functionalized AgNPs were also studied *in vitro* using a fibroblast cell line to determine changes in cytotoxicity for mammalian cells subjected to those concentrations that demonstrated antimicrobial efficacy. Conflicting reports have shown a significant range of cytotoxic effects on cells in the presence of AgNPs in both *in vitro* and *in vivo* models.[20, 23, 67, 70, 71, 75-77, 85, 87, 88] Recent review articles describe these findings in detail with respect to AgNP size, shape, surface functionalization, concentration, and stability, among other properties.[18, 20, 25, 34, 47, 49, 67] Our studies are conducted with 40 nm AgNPs, a size shown to be small enough to provide antimicrobial efficacy. However in a variety of studies,

their size was also considered to be within a range to mitigate cytotoxic effects in cells.[71] The concentration range selected for our study was based upon recent studies and the antimicrobial assays we performed. The maximum AgNP concentration we studied, 5.25 µg/ml, is notably lower compared to many literature reports.[18, 22, 71, 77, 83] We attribute this favorable outcome to our novel protein self-assembly AgNP functionalization technique which offers enhanced stability without significantly altering AgNP size. Greater stability allows for maintaining or increasing their antimicrobial properties, while provided the added benefit of reducing their cytotoxic effects.

We followed the morphological changes for the NIH/3T3 fibroblast cells by bright-field imaging following a 24 hour treatment with functionalized and control (citrate-coated) AgNPs. Adherent cells were imaged prior to treatment to ensure uniform confluency and morphology across the plates. A representative image is provided in Figure 5 which displays the brightfield image for a cells-only control well (sham treated, no AgNPs) following a 24 hour incubation.

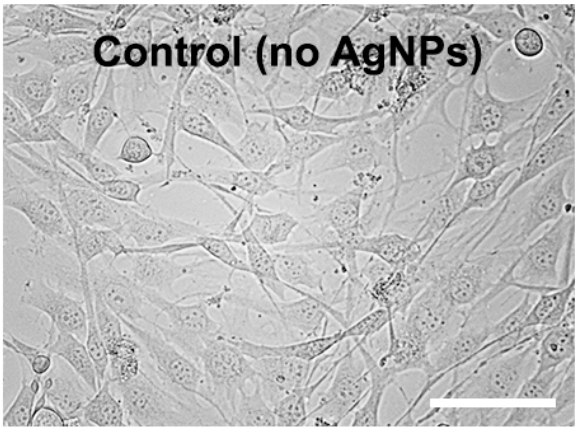

Figure 5. Brightfield imaging of the NIH/3T3 fibroblast cells control (no AgNPs) following a 24 hour incubation. Image is shown at 20X magnification; scale bar represents 100µm.

The morphological changes in the cells following the 24 hour incubation with 0.66 and 1.31 µg/mL citrate and GFP-AgBP-coated AgNPs treatments are shown in Figure 6. These

images can be directly compared to Figure 5 (cells-only control) as well as the higher concentrations of 2.63 and 5.25 µg/mL coated-AgNPs (Figure 7).

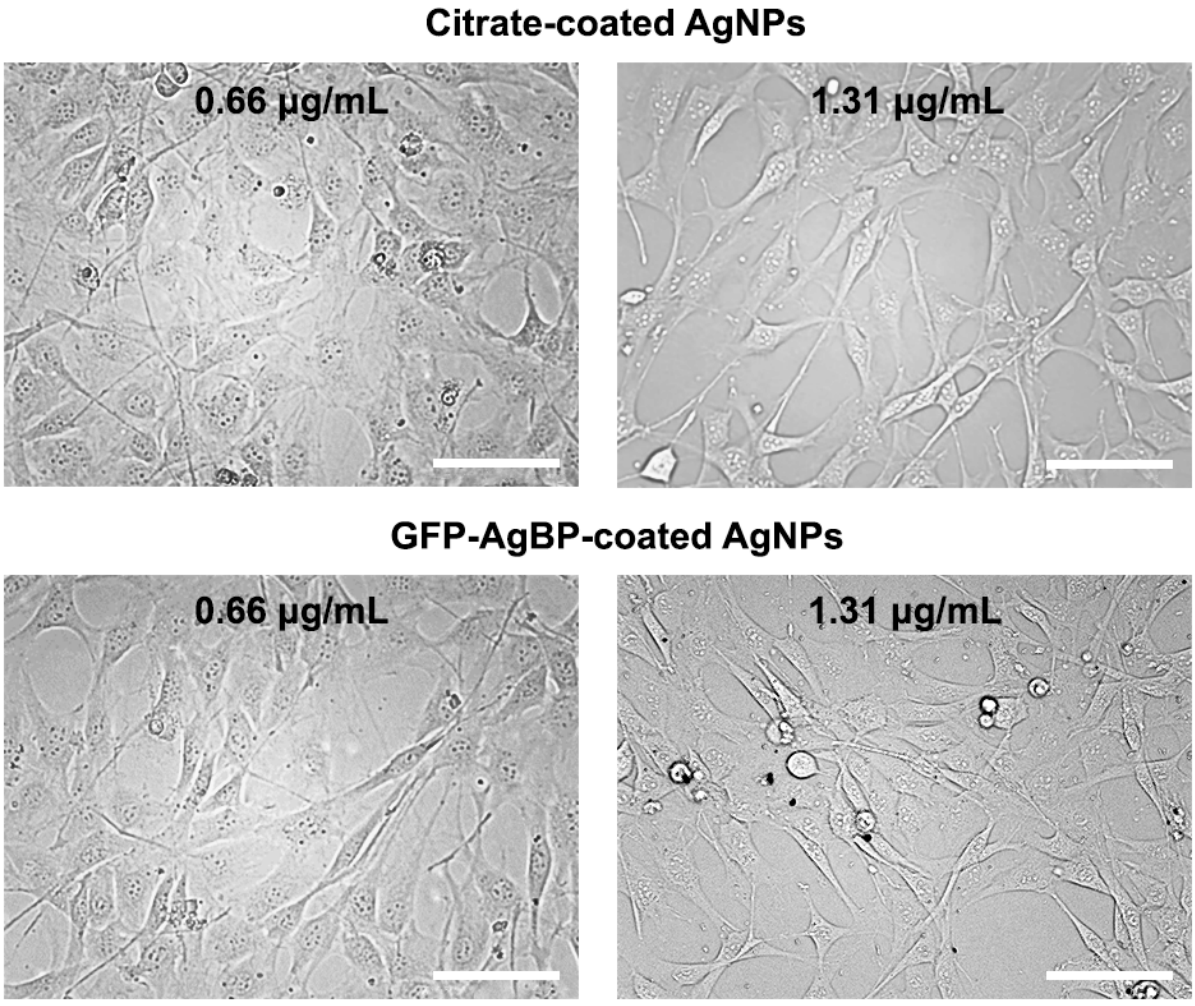

Figure 6. Representative brightfield images of the NIH/3T3 fibroblast cells treated with GFP-AgBP- or citrate-coated AgNPs at concentrations of 0.66 and 1.31 µg/mL. Following a 24 hour incubation, the cells appear relatively healthy for the lowest concentration (0.66 µg/mL) for both treatments as compared to the cells-only control shown in Figure 5. However, as AgNP concentration is increased to 1.31 µg/mL, cells appear to have an altered morphology and begin to detatch more significantly in the citrate-coated AgNPs as compared to the GFP-AgBP-coated AgNPs. Images are shown at 20X magnification; scale bar represents 100µm.

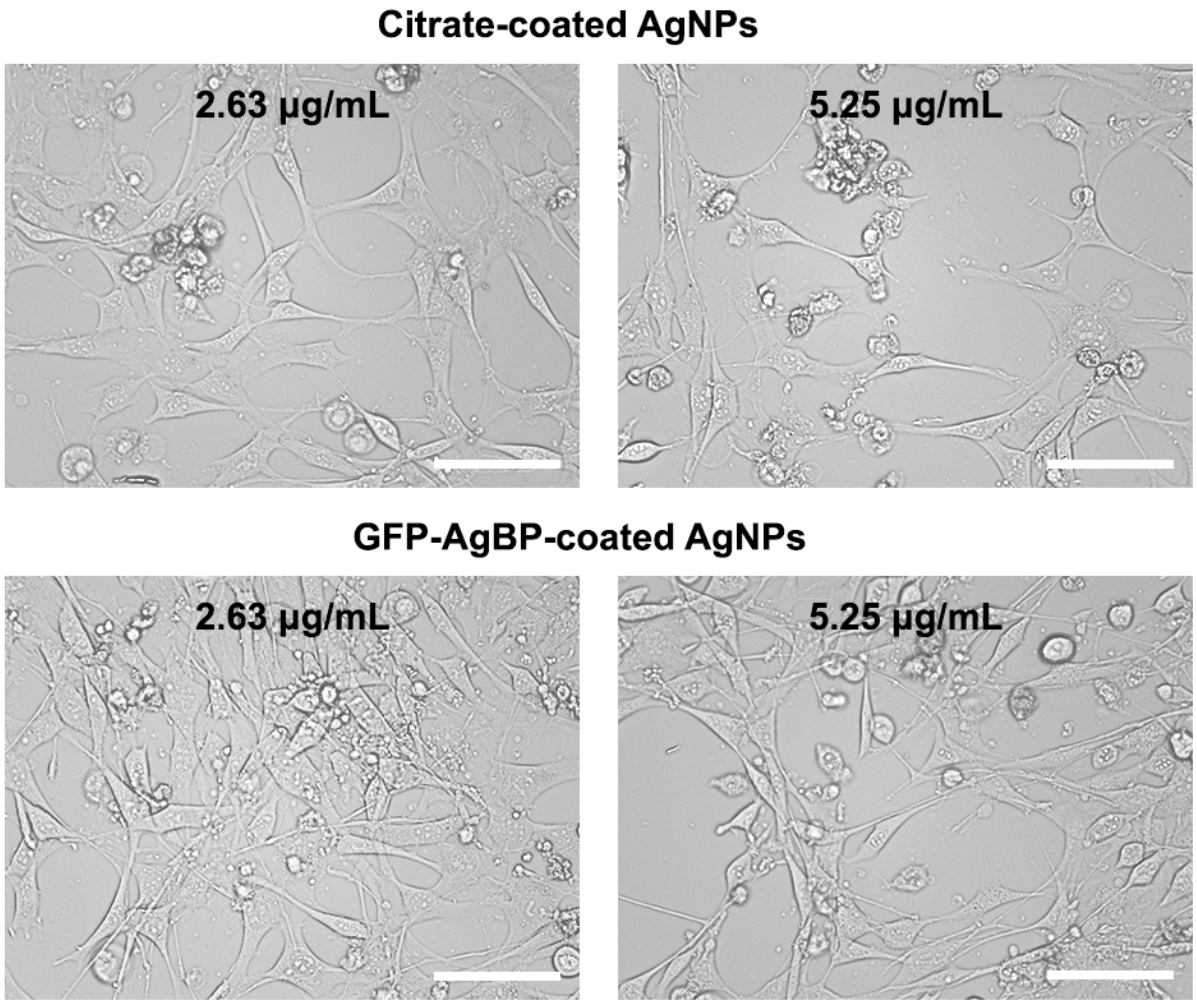

Figure 7. Brightfield imaging of the NIH/3T3 fibroblast cells treated with GFP-AgBP-coated (bottom) or citrate-coated (top) AgNPs at concentrations of 2.63 and 5.25 µg/mL. Following a 24 hour incubation, the cells appear less elongated and are seen to detach as AgNP concentration is increased (lower concentrations and control cells are shown in Figures 6 and 5, respectively). The morphological effects appear significantly less severe for GFP-AgBP-coated AgNPs as compared to stock AgNPs at the concentrations shown. Images are shown at 20X magnification; scale bar represents 100µm

In all concentrations, cells subjected to the stock, citrate-coated nanoparticles appeared to have a less-healthy cell morphology, as compared to cell treated with respective concentrations

of GFP-AgBP protein-coated AgNPs. As expected, cells appeared more viable and healthy at the lower AgNP concentrations. The number of adherent cells still remaining in each well was also concentration dependent, suggesting that the higher concentrations were more cytotoxic leading to an increase in cellular detachment due to their significantly reduced viability.

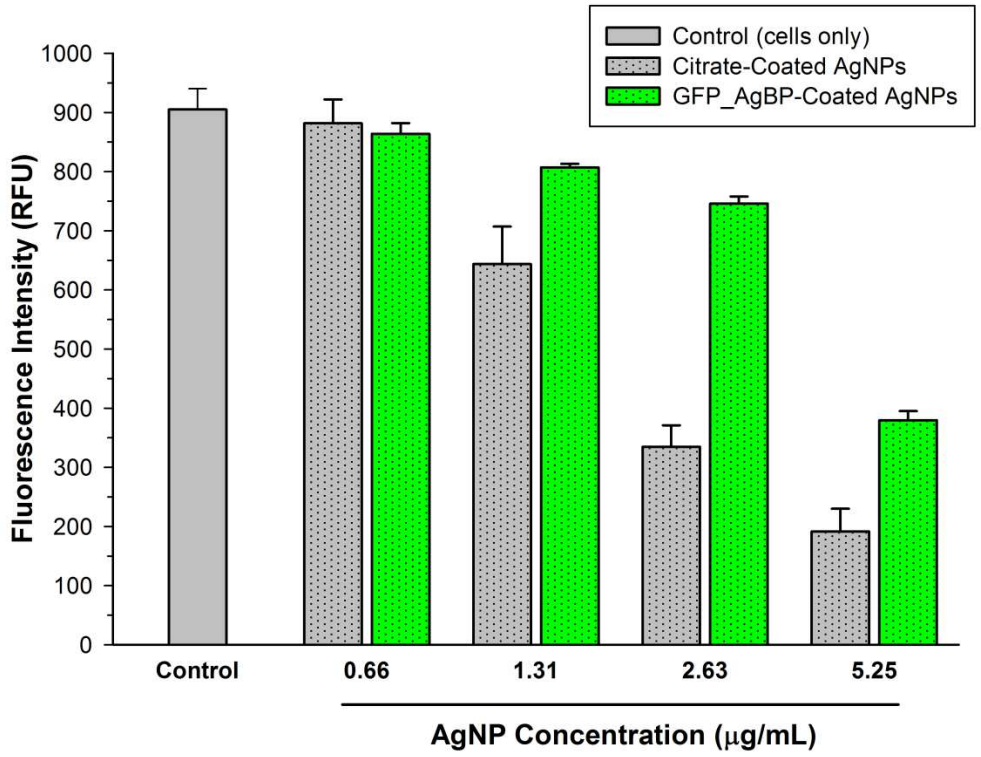

Figure 8. Cell viability of NIH/3T3 fibroblast cells exposed to increasing concentrations of AgNPs that are coated with either GFP-AgBP or citrate (control). There is a decreasing trend for cellular viability, measured by AlamarBlue fluorescence activity, as AgNP concentrations increase. Cells incubated with AgNPs functionalized with GFP-AgBP maintain a significantly higher cellular viability compared to cells exposed to citrate-coated AgNPs at corresponding concentrations (for concentrations of 1.31 μg/mL and greater).

In parallel, cellular viability was studied using two independent methods. The Live/Dead staining technique uses a green versus red fluorescent imaging to indicate cell viability and cytotoxicity, respectively. Because our engineered fusion protein featured GFP, each plate prior to Live/Dead staining was imaged and the fluorescent contribution of our GFP protein subtracted from the live-dead assay. Moreover, to confirm cellular viability, parallel studies were performed where treated cells were subjected to the AlamarBlue viability assay. Figure 8 shows average fluorescence intensity measurements from AlamarBlue treated wells. A concentration-dependent decrease in cellular viability was observed with increasing AgNP concentrations for both the citrate-coated and GFP-AgBP functionalized nanoparticle treatments. Further, we observed a statistically significant improvement in cellular viability for cells treated with protein-functionalized AgNPs as compared to stock, citrate-coated AgNPs at concentrations of 1.31, 2.63, and 5.25 μg/ml.

Comparable viability results were observed for treated cells analyzed using Live/Dead staining methods. Representative Live/Dead staining images shown in Figures 9 and 10 demonstrate the improved cellular viability and reduced cytotoxicity for protein-functionalized AgNPs as compared to citrate-coated controls at all AgNP concentrations. NIH/3T3 cells treated with GFP-AgBP-functionalized AgNPs measured greater viability and enhanced surface coverage more similar to the cell-only (untreated) control wells compared to citrate-coated nanoparticles at equal concentrations. Red fluorescent intensity, which indicates compromised membrane integrity and increasing cytotoxicity, increased with greater AgNP concentrations. However, cells treated with the protein-stabilized AgNPs show a significant reduction in cytotoxic activity at each concentration when compared to citrate-coated AgNP controls. The enhanced viability of cells exposed to GFP-AgBP-stabilized nanoparticles, as indicated by the green fluorescence intensity, demonstrates a clear dependence on AgNP surface functionalization for AgNPs of the same size and concentration, a finding reflected within the vast number of related publications.

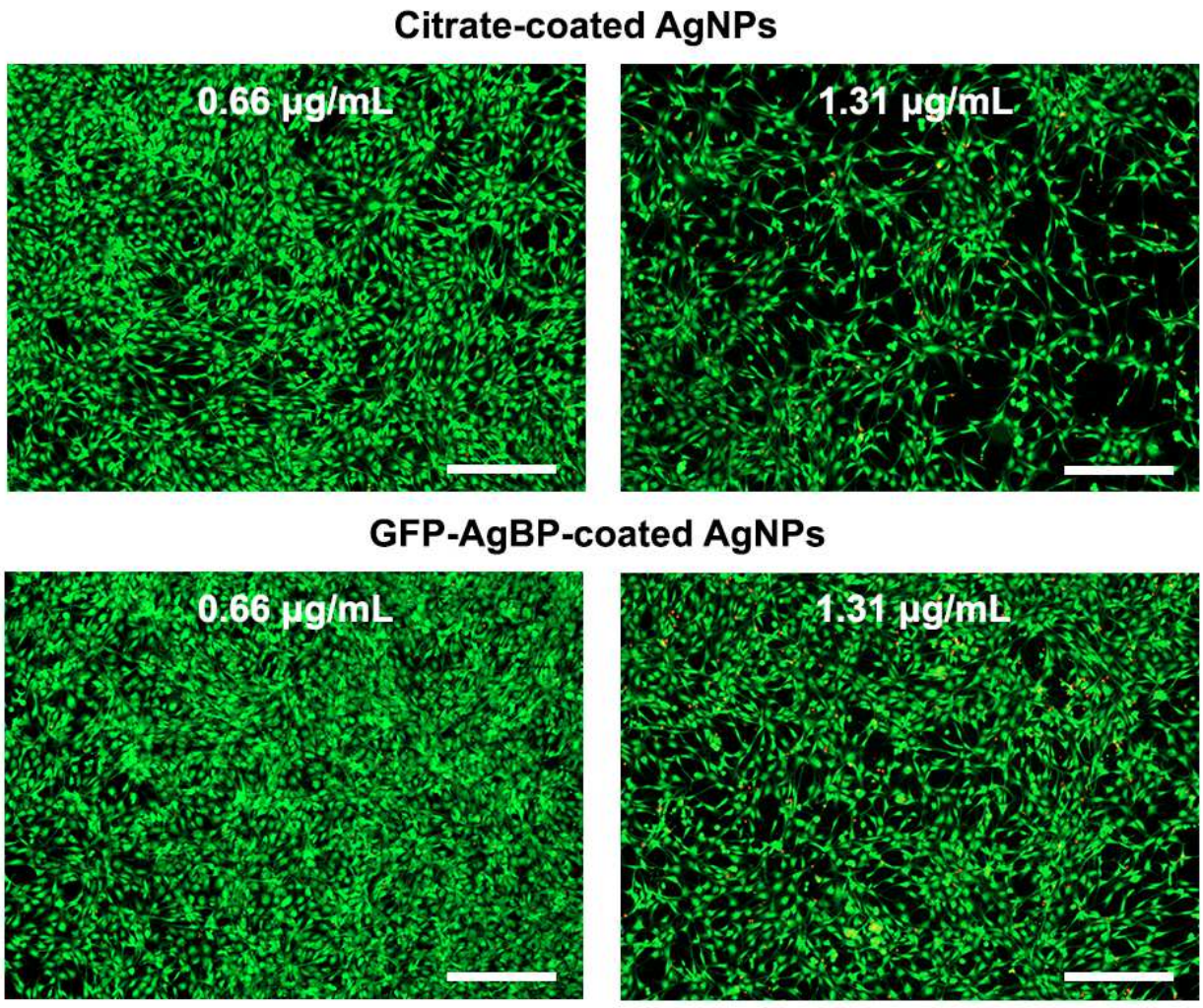

Figure 9. Representative fluorescence images of the NIH/3T3 fibroblast cells treated with GFP-AgBP- or citrate-coated AgNPs at 0.66 and 1.31 µg/mL concentrations by Live/Dead staining. Following a 24 hour incubation with AgNP treatments, viable cells are identified by their green stain and cellular cytotoxicity is indicated by red stain. Protein-functionalized AgNPs appear to maintain a significantly greater viability throughout increased concentrations as compared to cells treated with respective citrate-coated AgNPs. Images are shown at 4X magnification; scale bar represents 300µm.

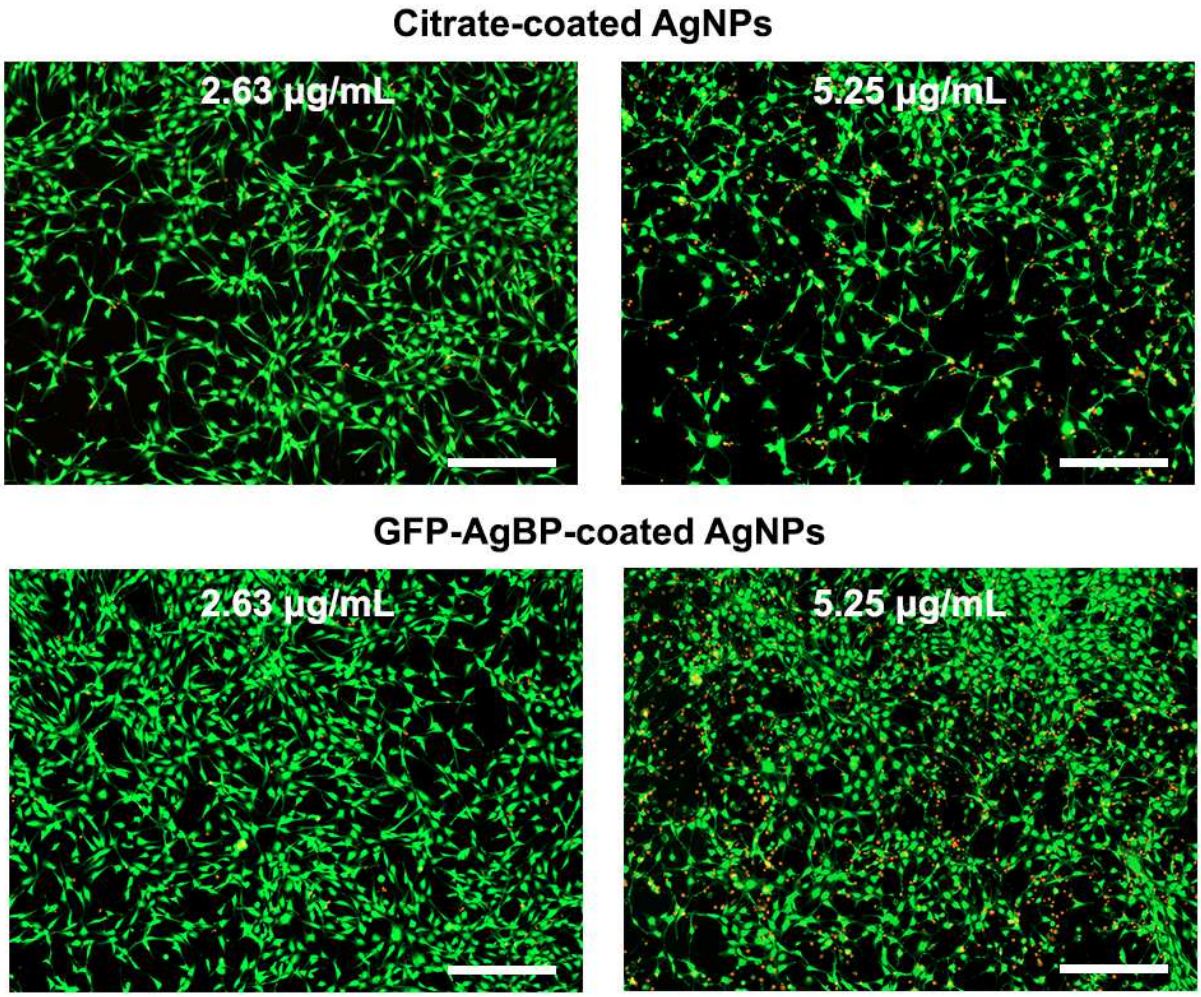

Figure 10. Representative fluorescence images of the NIH/3T3 fibroblast cells following a 24 hour treatment with either GFP-AgBP- or citrate-coated AgNPs at 2.63 and 5.25 µg/mL concentrations by Live/Dead staining. Cellular viability (green stain) reduces as AgNP concentration is increased (lower concentrations shown in Figure 9). However, protein-functionalized AgNPs maintain a greater viability throughout increased concentrations as compared to citrate-coated AgNPs. Cytotoxicity, indicated by the red fluorescence, was significantly greater (measured as a ratio to the number of viable cells/well) with increasing concentrations for citrate-coated compared to GFP-AgBP-coated AgNPs. Images are shown at 4X magnification; scale bar represents 300µm.

In this study, functionalized AgNPs were demonstrated to provide enhanced stability and reduced cytotoxic effects while still maintaining bactericidal efficiency. Our proposed approach using a peptide with specific inorganic-binding affinity offers the potential to engineer unique fusion proteins to provide tunable and predictable properties at the nanoparticle surface for enhanced biomaterial design toward reducing the burden of infection-associated implant failure in medical and dental devices.

4. Chapter 4: Conclusions

4.1 Conclusions

While studying biological interactions with the nanoscaled materials are extremely important to address their safety concern, these analyses are often still deficient for studies with silver nanoparticles. Silver nanoparticles offer an exceptional opportunity to combat infections and treat antibiotic resistant bacteria, but their widespread use has been limited because of unanswered questions regarding toxicity to host cells and the related protein complexes that create a corona on their surfaces. The protein corona confounds quantitative and qualitative analysis. One way to overcome these complex interactions may be to engineer the silver nanoparticle surface using biological self-assembly to provide a competitive advantage over other competitive absorption at the interface. Combinatorial-selected inorganic binding peptides may offer an opportunity to provide a relatively stable interface at the AgNP surfaces that better serves a biomedical application. Herein, we genetically engineered a silver binding peptide and used it to form a biointerface to stabilize the surface of AgNP. By providing the peptide tag to bind silver within the multifunctional protein complex we succeeded in creating a protein cage around the nanoparticle where the resulting interface may have a better chance to stand the complex ongoing biological interactions. GFP-AgBP fusion protein demonstrates its ability to bio-self-assemble onto AgNPs in a tunable, concentration-dependent manner and displays a strong binding stability. Our results showed that a low concentration of 40nm silver nanoparticles, stabilized with our engineered fusion protein, provide a local antibacterial efficacy at a suitably low concentration while mitigating the cytotoxicity and improving viability in a fibroblast cell model, *in vitro*. These results offer a one-step, environmentally friendly, and biomimetic approach to nanoparticle functionalization to overcome biomaterial-associated infection or offer a management path to the treatment of biofilm infected wounds.

References

1. Darouiche, R.O., *Device-associated infections: a macroproblem that starts with microadherence.* Clinical Infectious Diseases, 2001. **33**(9): p. 1567-1572.
2. Ventola, C.L., *Challenges in evaluating and standardizing medical devices in health care facilities.* P T, 2008. **33**(6): p. 348-59.
3. Besinis, A., et al., *Review of nanomaterials in dentistry: interactions with the oral microenvironment, clinical applications, hazards, and benefits.* ACS Nano, 2015. **9**(3): p. 2255-89.
4. Campoccia, D., L. Montanaro, and C.R. Arciola, *A review of the clinical implications of anti-infective biomaterials and infection-resistant surfaces.* Biomaterials, 2013. **34**(33): p. 8018-29.
5. Xuedong, Z., *Dental Caries: Principles and Management*. 2015: Springer Berlin Heidelberg.
6. Fernandes, J.M.F.A., et al., *Improving Antimicrobial Activity of Dental Restorative Materials*. Emerging Trends in Oral Health Sciences and Dentistry. 2015.
7. Gaviria, L., et al., *Current trends in dental implants.* J Korean Assoc Oral Maxillofac Surg, 2014. **40**(2): p. 50-60.
8. Costerton, J.W., P.S. Stewart, and E.P. Greenberg, *Bacterial biofilms: a common cause of persistent infections.* Science, 1999. **284**(5418): p. 1318-22.
9. Oh, C., et al., *Comparison of the Oral Microbiomes of Canines and Their Owners Using Next-Generation Sequencing.* PLoS One, 2015. **10**(7): p. e0131468.
10. Gallo, J., M. Holinka, and C.S. Moucha, *Antibacterial surface treatment for orthopaedic implants.* International Journal of Molecular Sciences, 2014. **15**(8): p. 13849-13880.
11. Zimmerli, W. and A. Trampuz, *Biomaterial-Associated Infection: A Perspective from the Clinic*, in *Biomaterials Associated Infection: Immunological Aspects and Antimicrobial Strategies*, F.T. Moriarty, A.J.S. Zaat, and J.H. Busscher, Editors. 2013, Springer New York: New York, NY. p. 3-24.
12. CDC, *Antibiotic Resistance Threats in the United States*. 2013, Centers for Disease Control and Prevention: Atlanta, GA, USA.
13. Spellberg, B., et al., *The Epidemic of Antibiotic-Resistant Infections: A Call to Action for the Medical Community from the Infectious Diseases Society of America.* Clinical Infectious Diseases, 2008. **46**(2): p. 155-164.
14. WHO, *Antimicrobial Resistance: Global Report on Surveillance*. 2014, World Health Organization: Geneva, Switzerland.
15. Ventola, C.L., *The Antibiotic Resistance Crisis: Part 1: Causes and Threats.* Pharmacy and Therapeutics, 2015. **40**(4): p. 277-283.
16. Brooks, B.D., A.E. Brooks, and D.W. Grainger, *Antimicrobial Medical Devices in Preclinical Development and Clinical Use*, in *Biomaterials Associated Infection: Immunological Aspects and Antimicrobial Strategies*, F.T. Moriarty, A.J.S. Zaat, and J.H. Busscher, Editors. 2013, Springer New York: New York, NY. p. 307-354.

17. Alexander, J.W., *History of the medical use of silver.* Surgical infections, 2009. **10**(3): p. 289-292.

18. Corrêa, J.M., et al., *Silver Nanoparticles in Dental Biomaterials.* International Journal of Biomaterials, 2015. **2015**: p. 485275.

19. Dallas, P., V.K. Sharma, and R. Zboril, *Silver polymeric nanocomposites as advanced antimicrobial agents: classification, synthetic paths, applications, and perspectives.* Advances in Colloid and Interface Science, 2011. **166**(1-2): p. 119-35.

20. dos Santos, C.A., et al., *Silver nanoparticles: therapeutical uses, toxicity, and safety issues.* Journal of Phamaceutical Sciences, 2014. **103**(7): p. 1931-44.

21. Duran, N., et al., *Silver nanoparticles: A new view on mechanistic aspects on antimicrobial activity.* Nanomedicine: Nanotechnology, Biology, and Medicine, 2016. **12**(3): p. 789-99.

22. Espinosa-Cristobal, L.F., et al., *Antibacterial effect of silver nanoparticles against Streptococcus mutans.* Materials Letters, 2009. **63**(29): p. 2603-2606.

23. Hernandez-Sierra, J.F., et al., *In vitro cytotoxicity of silver nanoparticles on human periodontal fibroblasts.* Journal of Clinical Pediatric Denstiry, 2011. **36**(1): p. 37-41.

24. Lu, Z., et al., *Size-dependent antibacterial activities of silver nanoparticles against oral anaerobic pathogenic bacteria.* Journal of Materials Science: Materials in Medicine, 2013. **24**(6): p. 1465-71.

25. Marin, S., et al., *Applications and toxicity of silver nanoparticles: a recent review.* Current Topics in Medicinal Chemistry, 2015. **15**(16): p. 1596-604.

26. Martinez-Castanon, G.A., et al., *Synthesis and antibacterial activity of silver nanoparticles with different sizes.* Journal of Nanoparticle Research, 2008. **10**(8): p. 1343-1348.

27. Monteiro, D.R., et al., *The growing importance of materials that prevent microbial adhesion: antimicrobial effect of medical devices containing silver.* International Journal of Antimicrobial Agents, 2009. **34**(2): p. 103-110.

28. Morones, J.R., et al., *The bactericidal effect of silver nanoparticles.* Nanotechnology, 2005. **16**(10): p. 2346-2353.

29. Pelgrift, R.Y. and A.J. Friedman, *Nanotechnology as a therapeutic tool to combat microbial resistance.* Advanced Drug Delivery Reviews, 2013. **65**(13-14): p. 1803-1815.

30. Rai, M., A. Yadav, and A. Gade, *Silver nanoparticles as a new generation of antimicrobials.* Biotechnology Advances, 2009. **27**(1): p. 76-83.

31. Rai, M.K., et al., *Silver nanoparticles: the powerful nanoweapon against multidrug-resistant bacteria.* Journal of Applied Microbiology, 2012. **112**(5): p. 841-852.

32. Sotiriou, G.A. and S.E. Pratsinis, *Antibacterial activity of nanosilver ions and particles.* Environmental Science & Technology, 2010. **44**(14): p. 5649-54.

33. Sotiriou, G.A. and S.E. Pratsinis, *Engineering nanosilver as an antibacterial, biosensor and bioimaging material.* Current Opinion in Chemical Engineering, 2011. **1**(1): p. 3-10.

34. Wei, L., et al., *Silver nanoparticles: synthesis, properties, and therapeutic applications.* Drug Discovery Today, 2015. **20**(5): p. 595-601.

35. Sondi, I. and B. Salopek-Sondi, *Silver nanoparticles as antimicrobial agent: a case study on E. coli as a model for Gram-negative bacteria.* Journal of colloid and interface science, 2004. **275**(1): p. 177-182.

36. Allaker, R.P. and K. Memarzadeh, *Nanoparticles and the control of oral infections.* International Journal of Antimicrobial Agents, 2014. **43**(2): p. 95-104.

37. Khan, S.T., J. Musarrat, and A.A. Al-Khedhairy, *Countering drug resistance, infectious diseases, and sepsis using metal and metal oxides nanoparticles: Current status.* Colloids and Surfaces B: Biointerfaces, 2016. **146**: p. 70-83.

38. Durán, N., G. Nakazato, and A.B. Seabra, *Antimicrobial activity of biogenic silver nanoparticles, and silver chloride nanoparticles: an overview and comments.* Applied Microbiology and Biotechnology, 2016: p. 1-16.

39. Mftah, A., et al., *Physicochemical properties, cytotoxicity, and antimicrobial activity of sulphated zirconia nanoparticles.* International Journal of Nanomedicine, 2015. **10**: p. 765-74.

40. Wang, J., et al., *Antibacterial Surface Design of Titanium-Based Biomaterials for Enhanced Bacteria-Killing and Cell-Assisting Functions Against Periprosthetic Joint Infection.* ACS Applied Materials & Interfaces, 2016. **8**(17): p. 11162-78.

41. Ren, G., et al., *Characterisation of copper oxide nanoparticles for antimicrobial applications.* International journal of antimicrobial agents, 2009. **33**(6): p. 587-590.

42. Azam, A., et al., *Antimicrobial activity of metal oxide nanoparticles against Gram-positive and Gram-negative bacteria: a comparative study.* International journal of nanomedicine, 2012. **7**: p. 6003.

43. Padmavathy, N. and R. Vijayaraghavan, *Enhanced bioactivity of ZnO nanoparticles—an antimicrobial study.* Science and Technology of Advanced Materials, 2008. **9**(3): p. 035004.

44. Lynch, I. and K.A. Dawson, *Protein-nanoparticle interactions.* Nano Today, 2008. **3**(1-2): p. 40-47.

45. Yucesoy, D.T., et al., *Chimeric peptides as implant functionalization agents for titanium alloy implants with antimicrobial properties.* JOM (1989), 2015. **67**(4): p. 754-766.

46. Yazici, H., et al., *Engineered Chimeric Peptides as Antimicrobial Surface Coating Agents toward Infection-Free Implants.* ACS Appl Mater Interfaces, 2016. **8**(8): p. 5070-81.

47. Durán, N., et al., *Silver nanoparticle protein corona and toxicity: a mini-review.* Journal of Nanobiotechnology, 2015. **13**: p. 55.

48. Hall Sedlak, R., et al., *Engineered Escherichia coli Silver-Binding Periplasmic Protein That Promotes Silver Tolerance.* Applied and Environmental Microbiology, 2012. **78**(7): p. 2289-2296.

49. Lee, Y.K., et al., *Effect of the protein corona on nanoparticles for modulating cytotoxicity and immunotoxicity.* International Journal of Nanomedicine, 2015. **10**: p. 97-113.

50. Monopoli, M.P., et al., *Biomolecular coronas provide the biological identity of nanosized materials.* Nature Nanotechnology, 2012. **7**(12): p. 779-86.

51. Graf, P., et al., *Silicification of Peptide-Coated Silver Nanoparticles—A Biomimetic Soft Chemistry Approach toward Chiral Hybrid Core−Shell Materials.* ACS Nano, 2011. **5**(2): p. 820-833.

52. Ruden, S., et al., *Synergistic interaction between silver nanoparticles and membrane-permeabilizing antimicrobial peptides.* Antimicrobial Agents and Chemotherapy, 2009. **53**(8): p. 3538-40.

53. Carmona-Ribeiro, A.M. and L.D. de Melo Carrasco, *Cationic Antimicrobial Polymers and Their Assemblies.* International Journal of Molecular Sciences, 2013. **14**(5): p. 9906-9946.

54. Munoz-Bonilla, A. and M. Fernández-García, *Polymeric materials with antimicrobial activity.* Progress in Polymer Science, 2012. **37**(2): p. 281-339.

55. Gottenbos, B., et al., *Antimicrobial effects of positively charged surfaces on adhering Gram-positive and Gram-negative bacteria.* Journal of antimicrobial chemotherapy, 2001. **48**(1): p. 7-13.

56. Siedenbiedel, F. and J.C. Tiller, *Antimicrobial polymers in solution and on surfaces: overview and functional principles.* Polymers, 2012. **4**(1): p. 46-71.

57. Kenawy, E.-R., S. Worley, and R. Broughton, *The chemistry and applications of antimicrobial polymers: a state-of-the-art review.* Biomacromolecules, 2007. **8**(5): p. 1359-1384.

58. Timofeeva, L. and N. Kleshcheva, *Antimicrobial polymers: mechanism of action, factors of activity, and applications.* Applied microbiology and biotechnology, 2011. **89**(3): p. 475-492.

59. Mi, L. and S. Jiang, *Integrated antimicrobial and nonfouling zwitterionic polymers.* Angewandte Chemie International Edition, 2014. **53**(7): p. 1746-1754.

60. Jennings, M.C., K.P.C. Minbiole, and W.M. Wuest, *Quaternary Ammonium Compounds: An Antimicrobial Mainstay and Platform for Innovation to Address Bacterial Resistance.* ACS Infectious Diseases, 2015. **1**(7): p. 288-303.

61. McBain, A.J., et al., *Effects of quaternary-ammonium-based formulations on bacterial community dynamics and antimicrobial susceptibility.* Applied and environmental microbiology, 2004. **70**(6): p. 3449-3456.

62. Hegstad, K., et al., *Does the wide use of quaternary ammonium compounds enhance the selection and spread of antimicrobial resistance and thus threaten our health?* Microbial drug resistance, 2010. **16**(2): p. 91-104.

63. Demberelnyamba, D., et al., *Synthesis and antimicrobial properties of imidazolium and pyrrolidinonium salts.* Bioorganic & medicinal chemistry, 2004. **12**(5): p. 853-857.

64. Buffet-Bataillon, S., et al., *Emergence of resistance to antibacterial agents: the role of quaternary ammonium compounds—a critical review.* International journal of antimicrobial agents, 2012. **39**(5): p. 381-389.

65. Alberto, E.E., et al., *Imidazolium ionic liquids containing selenium: synthesis and antimicrobial activity.* Organic & biomolecular chemistry, 2011. **9**(4): p. 1001-1003.

66. Tran, P.A. and T.J. Webster, *Antimicrobial selenium nanoparticle coatings on polymeric medical devices.* Nanotechnology, 2013. **24**(15): p. 155101.

67. Sharma, V.K., et al., *Organic-coated silver nanoparticles in biological and environmental conditions: fate, stability and toxicity.* Advances in Colloid and Interface Science, 2014. **204**: p. 15-34.

68. Lankveld, D.P., et al., *The kinetics of the tissue distribution of silver nanoparticles of different sizes.* Biomaterials, 2010. **31**(32): p. 8350-61.

69. Powers, C.M., et al., *Silver nanoparticles compromise neurodevelopment in PC12 cells: critical contributions of silver ion, particle size, coating, and composition.* Environmental Health Perspectives, 2011. **119**(1): p. 37-44.

70. Yen, H.J., S.H. Hsu, and C.L. Tsai, *Cytotoxicity and immunological response of gold and silver nanoparticles of different sizes.* Small, 2009. **5**(13): p. 1553-61.

71. Gliga, A.R., et al., *Size-dependent cytotoxicity of silver nanoparticles in human lung cells: the role of cellular uptake, agglomeration and Ag release.* Particle and Fibre Toxicology, 2014. **11**: p. 11.

72. Pal, S., Y.K. Tak, and J.M. Song, *Does the antibacterial activity of silver nanoparticles depend on the shape of the nanoparticle? A study of the gram-negative bacterium Escherichia coli.* Applied and Environmental Microbiology, 2007. **73**(6): p. 1712-1720.

73. Johansson, I., et al., *The Microbiome in Populations with a Low and High Prevalence of Caries.* J Dent Res, 2016. **95**(1): p. 80-6.

74. Caufield, P.W., Y. Li, and A. Dasanayake, *Dental caries: an infectious and transmissible disease.* Compend Contin Educ Dent, 2005. **26**(5 Suppl 1): p. 10-6.

75. Braydich-Stolle, L.K., et al., *Silver nanoparticles disrupt GDNF/Fyn kinase signaling in spermatogonial stem cells.* Toxicological Sciences, 2010. **116**(2): p. 577-89.

76. Arora, S., et al., *Interactions of silver nanoparticles with primary mouse fibroblasts and liver cells.* Toxicology and Applied Pharmacology, 2009. **236**(3): p. 310-8.

77. Huang, Y., X. Lu, and J. Ma, *Toxicity of silver nanoparticles to human dermal fibroblasts on microRNA level.* Journal of Biomedical Nanotechnology, 2014. **10**(11): p. 3304-17.

78. Hsin, Y.H., et al., *The apoptotic effect of nanosilver is mediated by a ROS- and JNK-dependent mechanism involving the mitochondrial pathway in NIH3T3 cells.* Toxicology Letters, 2008. **179**(3): p. 130-139.

79. Miclaus, T., et al., *Dynamic protein coronas revealed as a modulator of silver nanoparticle sulphidation in vitro.* Nat Commun, 2016. **7**.

80. Hnilova, M., et al., *Multifunctional Protein-Enabled Patterning on Arrayed Ferroelectric Materials.* ACS Applied Materials & Interfaces, 2012. **4**(4): p. 1865-1871.

81. Yuca, E., et al., *In vitro labeling of hydroxyapatite minerals by an engineered protein.* Biotechnology and Bioengineering, 2011. **108**(5): p. 1021-30.

82. Podila, R., et al., *Effects of surface functional groups on the formation of nanoparticle-protein corona.* Applied Physics Letters, 2012. **101**(26): p. 263701.

83. Kujda, M., et al., *Charge Stabilized Silver Nanoparticles Applied as Antibacterial Agents.* Journal of Nanoscience and Nanotechnology, 2015. **15**(5): p. 3574-3583.

84. dos Santos, C.A., et al., *Antimicrobial effectiveness of silver nanoparticles co-stabilized by the bioactive copolymer pluronic F68.* Journal of Nanobiotechnology, 2012. **10**: p. 43-43.

85. Jiang-Jen, L., et al., *The cellular responses and antibacterial activities of silver nanoparticles stabilized by different polymers.* Nanotechnology, 2012. **23**(6): p. 065102.

86. Sivera, M., et al., *Silver Nanoparticles Modified by Gelatin with Extraordinary pH Stability and Long-Term Antibacterial Activity.* PLoS ONE, 2014. **9**(8): p. e103675.

87. He, W., et al., *In Vitro Effect of 30 nm Silver Nanoparticles on Adipogenic Differentiation of Human Mesenchymal Stem Cells.* Journal of Biomedical Nanotechnology, 2016. **12**(3): p. 525-35.

88. Yu, X., F. Hong, and Y.-Q. Zhang, *Bio-effect of nanoparticles in the cardiovascular system.* Journal of Biomedical Materials Research Part A, 2016: p. n/a-n/a.